JOURNAL OF MATERIALS SCIENCE: MATERIALS IN ELECTRONICS 1 (1990) 90–94

The NTC thermistor fabricated by boundary-layer technology

IN-CHYUAN HO, SHEN-LI FU
Department of Electrical Engineering, National Cheng Kung University, Tainan, Taiwan

A thermistor with a negative temperature coefficient of resistance (NTCR), based on the semiconducting $(Ba_{0.8}Sr_{0.2})(Ti_{0.9}Zr_{0.1})O_3$ ceramics, is fabricated by boundary-layer (BL) technology. By adding a suitable amount of V_2O_5 as additive, a semiconducting boundary layer is segregated at the grain boundaries after sintering in a reducing atmosphere. This layer dominates the temperature-dependent property and shows an NTCR effect with a thermistor constant of about 4200 K. Based on the microstructural and electrical properties, an n^+–n–n^+ energy band model is proposed for this boundary-layer thermistor.

1. Introduction

Grain-boundary phenomena in electronic ceramics have been widely studied to achieve various properties and applications over the last three decades [1–3]. These include insulators, varistors, positive temperature coefficient resistors (PTCRs) and capacitors. As is well known, secondary phases or impurities at grain boundaries either determine the grain growth during sintering, or influence the electrical properties. The most popular, for example, are the nonlinear current–voltage characteristics of ZnO varistors [2], and the high permittivity of $SrTiO_3$-based grain-boundary barrier layer (GBBL) capacitors [3]. The electrical characteristics of these BL devices are directly determined by the physical properties of the second-phase layers in the grain boundaries. However, the basic composition of these devices for semiconductive grains are different. From the previous work [4–6], the semiconducting $(Ba_{0.8}Sr_{0.2})(Ti_{0.9}M_{0.1})O_3$ ceramics (where M is tin or zirconium) are fabricated for barrier-layer device applications. The structure of the conventional BL devices is shown in Fig. 1 [7], which is composed of semiconductive grains separated by insulating layers at the grain boundaries. The thickness and resistivity of the insulating layers depend on the manufacturing process as well as the composition [1, 8].

Based on the above statements, it may be seen that the property of the boundary layer composition determines, at least to some extent, the property of the fabricated boundary layer devices. A new method of fabricating an NTC thermistor is thus proposed in this study by generating a temperature-sensitive boundary layer in the grain boundaries of the selected semiconductive ceramic substrate. The principle of the formation of an NTCR layer is to utilize the fact that a liquid phase is usually coated around the grains during sintering, which will segregate and form a grain-boundary layer as the temperature cools from the sintering temperature. In this paper, a boundary-layer NTC thermistor, which is fabricated by a one-stage sintering, together with its related properties, are reported.

2. Experimental procedure

Raw materials of reagent-grade $BaCO_3$, $SrCO_3$, TiO_2 and ZrO_2 (Merck) are weighed in appropriate proportions to prepare the composition of $(Ba_{0.8}Sr_{0.2})(Ti_{0.9}Zr_{0.1})O_3$ (BSZT) ceramics. Wet ball-milling is conducted for 4 h with distilled water as the medium. After drying, the mixed powders are calcined at 1150° C for 2 h. In this study, V_2O_5 is selected as the main constituent of the boundary-layer composition. Owing to its low melting point (690° C) [9] and the negative temperature coefficient characteristics of the resistivity of vanadate-pentoxide-based mixtures and the amorphism [10, 11], it is expected that a NTCR boundary layer will be obtained in the grain boundary of the BSZT ceramics.

A suitable amount of V_2O_5 is first blended with the calcined $(Ba_{0.8}Sr_{0.2})(Ti_{0.9}Zr_{0.1})O_3$ dielectric powder, then 0.2 wt % SiO_2 is added to promote sintering. The blended powder is pressed into disc-shaped samples of 14 mm diameter. Sintering conditions are set at 1380° C for 4 h in a reducing atmosphere (2% H_2 + 98% N_2) to achieve the semiconductive property with the desired microstructure. Furnace-cooling is conducted in the same atmosphere up to 900° C, and then cooled to room temperature in air. The microstructures of the sintered samples are examined by scanning electron microscopy (SEM), and the semi-quantitative analysis of elements is performed by energy dispersive spectrometry (EDS). In addition, line-scanning analysis is also undertaken to investigate the relative compositional fluctuations in the grains as well as at the grain boundary.

For electrical measurements, the sintered specimens are polished to 1 mm thickness, and the In/Ga-containing silver paste is painted on both sides of the polished specimens as electrodes. The ohmic contact is confirmed from the linear current–voltage property examined using a curve tracer (Kikusui 5802). The temperature-dependent resistances are measured, using a digital multimeter (Keithley 175), in a temperature-programmable chamber. Resistivity is calculated from the measured resistance, electrode

0957–4522/90 $03.00 + .12 © *1990 Chapman and Hall Ltd.*

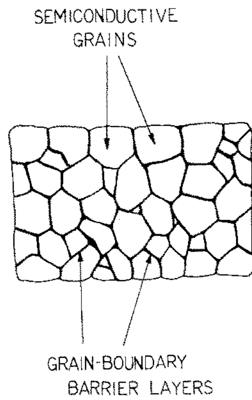

Figure 1 The ceramic structures of conventional boundary-layer devices [7].

area, and thickness of the specimen. For investigating the effect of additives, the d.c. current–voltage characteristics are determined for samples with different additive contents.

3. Results

3.1. The negative TCR properties

Fig. 2 shows the variations of electrical resistivity with respect to temperature for the BSZT-based ceramics sintered in 98% N_2 + 2% H_2 atmosphere. The pure, the tantallum-doped, and the nobium-doped specimens all show a diminished PTCR property with low bulk resistivity. This is attributed to the compensation of metal vacancies by oxygen vacancies, as is known from the reducing experiment on barium titanate [12, 13]. On the other hand, the 0.2 mol % V_2O_5-doped specimen shows a negative TCR effect with high room-temperature resistivity. An increased potential barrier is thus formed at the grain boundary. Because the switching property of resistance in VO_2 at a temperature near its Curie point (about 67° C) is not found, the semiconductor–metal transition [14] does not apparently occur here. That is, the vanadium pentoxide was not reduced to VO_2, whereas the formation of V_2O_{5-x} $(x < 1)$ is most likely in this experiment to explain its semiconducting property, caused by electron hopping between V^{4+} and V^{5+} [15].

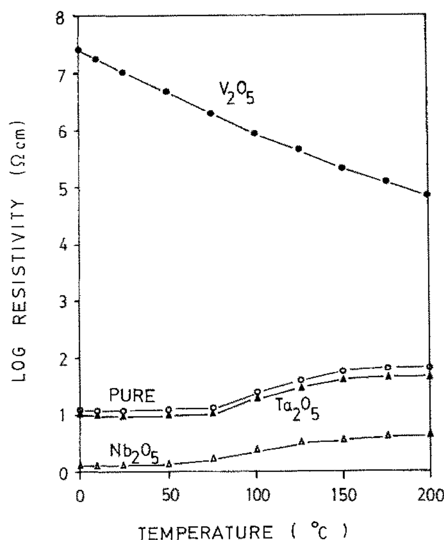

Figure 2 The variations of resistivity with temperature for the BSZT-based ceramics sintered at 1380° C in 98% N_2 + 2% H_2. The amount of each dopant denoted is 0.2 mol %.

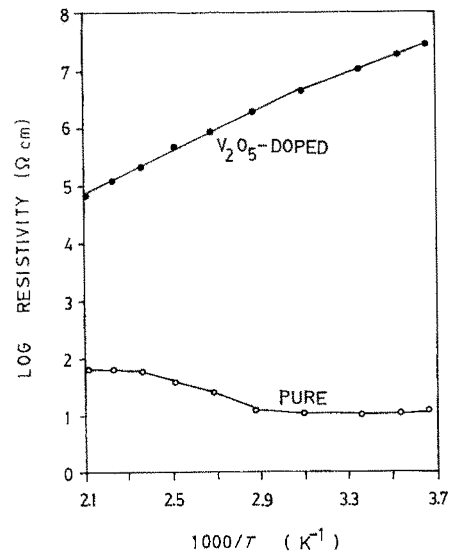

Figure 3 Arrhenius plots of resistivity for the pure and 0.2 mol % V_2O_5-doped BSZT ceramics in Fig. 2.

If the Arrhenius plots for the V_2O_5-doped specimen in Fig. 2 are drawn, as shown in Fig. 3, the thermistor constant B can be obtained according to the relationship

$$R(T) = R_0 \exp\left[B\left(\frac{1}{T} - \frac{1}{T_0}\right)\right] \quad (1)$$

where $R(T)$ and R_0 are the resistances of the thermistor measured at absolute temperature T and at reference temperature T_0, respectively. As calculated, B is 4200 K for temperatures above 50° C, while it is slightly lower for temperatures below 25° C. This might be attributable to the effect of tetragonal-cubic phase

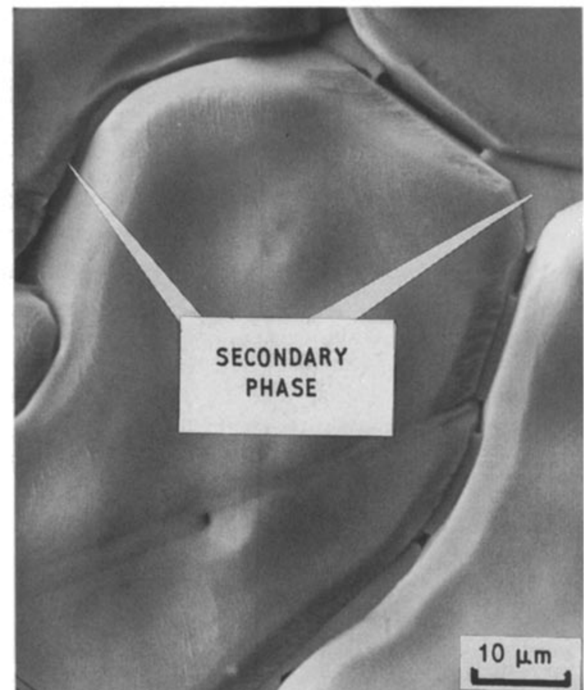

Figure 4 Scanning electron micrograph of the 0.4 mol % V_2O_5-doped BSZT ceramics. Secondary phase is distributed at the grain boundaries.

TABLE I The EDS analysis of the grains and boundary layer in the 0.4 mol % V_2O_5-doped BSZT ceramics, sintered at 1380° C in a 98% N_2 + 2% H_2 atmosphere. Data for grains I and II are detected from two different grains

	(at %)						
	Ba	Sr	Zr	Ti	V	Si	Al
Boundary layer	69.22	1.12	0.57	0.28	27.49	1.31	0.01
Grain I	38.57	10.40	5.44	45.43	0.02	0.12	0.02
Grain II	38.30	11.17	5.31	44.93	0.08	0.21	0

transition of the BSZT ceramics, because the Curie temperature of $(Ba_{0.8}Sr_{0.2})(Ti_{0.9}Zr_{0.1})O_3$ ceramics is around 34° C [16], with a somewhat diffused phase transition due to the incorporation of zirconium [17]. If the diffused phase transition is enhanced by raising the temperature, the gradually disappearing spontaneous polarization might increase the activation energy at the interface between the grain and the boundary layer, and this causes the higher thermistor constant.

3.2. Microstructure and energy band model

A scanning electron micrograph of the free surface for the 0.4 mol % V_2O_5-doped specimen sintered at 1380° C in a 98% N_2 + 2% H_2 atmosphere, is shown in Fig. 4. The secondary phase is found to be distributed in the grain boundaries, as well as in the intergranular junctions. EDS analysis shows that the second-phase layer mainly consists of barium and vanadium. In addition, small amounts of strontium, zirconium, silicon and aluminium are also detected, as listed in Table I. The source of aluminium might be from the process of ball-milling. Although the semi-quantitative analysis of EDS might cause some deviations, the line-scanning analysis on the grains and grain boundary, as shown in Fig. 5, also indicates a barium-rich and vanadium-containing second-phase layer.

It is known that several compounds such as $Ba_2V_2O_7$ and $Ba_3V_2O_8$ (nBaO · V_2O_5) can be formed from the reaction between BaO and V_2O_5 [18]. Similarly, compounds of nSrO · V_2O_5 can also be formed between SrO and V_2O_5 [19]. As the lowest melting points for $Ba_3V_2O_8$ and $Sr_3V_2O_8$ are 1100 and 1250° C [18, 19], respectively, enhanced grain growth is obtained due to the liquid phases formed during sintering. With lower BaO content, the melting point is lower [18] and the flux tends either to segregate at the intergranular junctions, or to vapourize during densification. On the other hand, for the flux with higher BaO content, which has a higher melting point, it will segregate at the grain boundaries as well as at the intergranular junctions. The atomic ratio of Ba/V for the second-phase layer calculated from Table I is 2.52, which is thought to be 5BaO · V_2O_5 with small amounts of SiO_2, SrO and ZrO_2. In addition, the pin-shaped titanium-rich secondary phase is also observed in the sintered specimens (not shown here), as usually found in TiO_2-rich barium titanate. With these properties, the non-stoichiometric deviations of the grains from the predetermined composition, as found in Table I, are understandable.

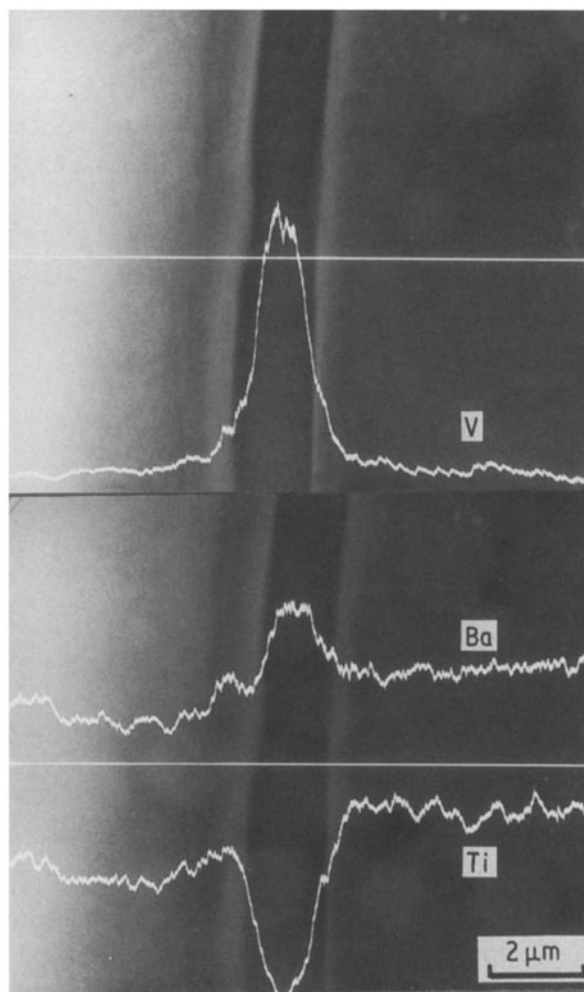

Figure 5 Line-scanning analysis of vanadium, barium and titanium in the 0.4 mol % V_2O_5-doped BSZT ceramics.

Because the secondary phase forms a barrier to the charge carriers which provide transport through semiconductive grains, the resistivity of the grain boundary is increased in comparison with the low-resistivity grains. The electrical property of such a boundary-layer structure can be expressed by an n^+–n–n^+ energy band model in equilibrium, as shown in Fig. 6, where E_s is the electron affinity difference between the semiconductive grain and the boundary layer, E_b the bending of the energy band caused by the trapping states (E_t) at the interfaces, E_c the lowest level of the conduction band, and E_f the Fermi level of the semiconductive grains. The semiconductive grain is known as n-type due to the electron accompanying the

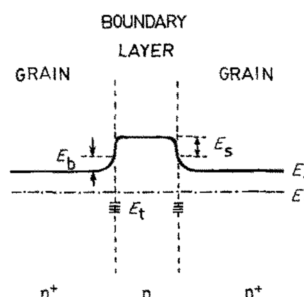

Figure 6 Energy band model of the BSZT-based NTC thermistor.

oxygen vacancy, as in the following reaction [20]

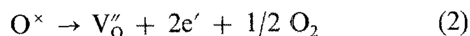

$$O^{\times} \rightarrow V_O'' + 2e' + 1/2\, O_2 \qquad (2)$$

From the pure-BSZT specimens sintered in a reducing atmosphere, the electron concentration in the semiconductive grains is estimated to be $10^{18}\,cm^{-3}$. Therefore, the low-resistivity grains are denoted by n^+, and the high-resistivity boundary layer by n. Most of the electrons drawn from the semiconductive grains are bound to the trapping states, while some of the electrons surmount the barrier and reach the conduction band of the boundary layer by diffusion, hence providing the transport current.

According to the Fermi distribution function

$$f(E) = \frac{1}{1 + \exp\,[(E - E_F)/KT]} \qquad (3)$$

where the value of $f(E)$ is the probability that the quantum state of energy E is occupied by an electron. From the Fermi distribution curves at different temperatures [21], it is known that the value of $f(E)$ for energy levels near the conduction band is increased at higher temperature. This leads to a larger increase in the concentration of thermionic emission carriers in the n-layer than in the n^+-grains, and the boundary-layer-dominated NTCR property is thus observed.

Further experiments for the mixed powders with compositions as listed in Table I show a melting point of about 1320° C. However, due to the poor mechanical strength of the sintered sample and the poor adhesion between its surface and the electrode, the electrical properties of the sintered second-phase ceramics are not available.

3.3. Effect of additive content

As the barrier-layer resistivity depends on the activation energy required to surmount the potential barrier, the resistivity of the thermistor can be expressed as [22]

$$\rho(T) = \rho_0 \exp\left(\frac{E_A}{KT}\right) \qquad (4)$$

where ρ_0 is a constant, K is the Boltzmann constant, and E_A is the activation energy, which might be attributed to many mechanisms, including grain-boundary potential (barrier height), small polaron hopping potential, band gap, deep-donor ionization energy, and ion hopping potential [23, 24]. However, the nearly equal slopes of the Arrhenius plots shown in Fig. 7 reveals that different amounts of additives result in almost the same activation energy (0.36 eV), and lower resistivity is obtained with smaller amounts of additive. Thus the barrier height of the boundary layer is almost independent of its thickness. However, the lower resistivity for specimens with smaller amounts of additives might be attributable to the thinner second-phase layer, which leads to a higher leakage current and lower breakdown voltage. That is, the tunnelling current might contribute at lower bias. The current–voltage characteristics of the thermistors with different amounts of additives are shown in Fig. 8, in which the specimen containing 0.2 mol % V_2O_5 shows

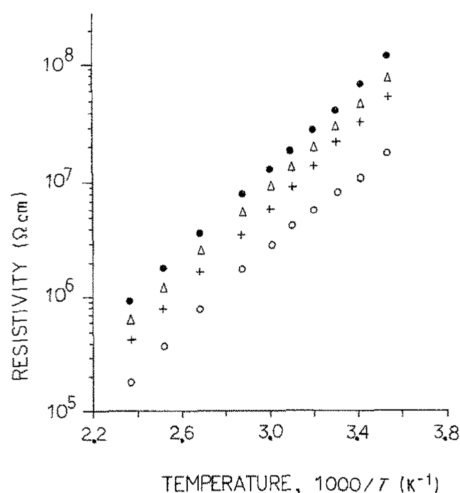

Figure 7 Arrhenius plots of the BSZT-based thermistors containing different amounts of V_2O_5: (○) 0.2 mol % (+) 0.4 mol %, (△) 0.6 mol %, (●) 0.8 mol %. Sintering is conducted at 1380° C in a 98% N_2 + 2% H_2 atmosphere.

a nonlinear current–voltage property when bias is increased to 10 V. This phenomenon agrees well with the explanation stated above. From this figure, one can conclude that the addition of more than 0.2 mol % V_2O_5 is essential for the thermistor to avoid the tunnelling effect, with which the thermistor will show a nonlinear current–voltage relationship.

If the hydrogen content in a reducing atmosphere is increased, or a small amount of cobalt oxide is added, the room-temperature resistance is expected to be lowered, with the thermistor constant kept above 3000. This is still under investigation.

4. Conclusion

NTC thermistors of BSZT-based ceramics are designed and fabricated by the boundary-layer technology, which was applied in the development of the BL capacitor. The main difference between the BL thermistor and the BL capacitor is the NTCR property of the semiconducting boundary layer, which replaces

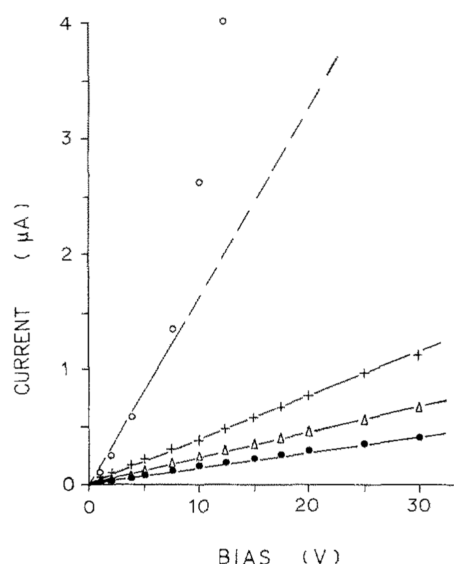

Figure 8 The current–voltage characteristics of the BSZT-based ceramics in Fig. 7. For key, see Fig. 7.

the insulating layer used in the BL capacitor. An n^+–n–n^+ energy band model is proposed for this boundary-layer thermistor.

The thermistor constant, B, of the V_2O_5-doped BSZT ceramics sintered in a reducing atmosphere is about 4200 K in this study. The resistance and breakdown voltage of the thermistor are dependent on the additives content; smaller amounts of additives lead to a lower resistance and lower breakdown voltage, while the thermistor constants are virtually unchanged. Addition of more than 0.2 mol % V_2O_5 is necessitated to avoid the tunnelling effect as well as a nonlinear current–voltage relationship.

References

1. W. D. KINGERY, "Advances in Ceramics", Vol. 1 (The American Ceramic Society, Columbus, Ohio, 1981) p. 1.
2. M. MATSUOKA, *Jpn J. Appl. Phys.* **10** (1971) 736.
3. A. YAMAJI and S. WAKU, *Rev. Electr. Commun. Lab.* **20** (1972) 747.
4. S. L. FU and S. Y. CHENG, in Proceedings of the 38th Electronic Components Conference (IEEE CHMT Society) Los Angeles (1988) p. 119.
5. S. L. FU, G. F. YANG and S. Y. CHENG, in Proceedings of the 5th International Microelectronics Conference, Tokyo (ISHM, Japan chapter) (1988) p. 201.
6. S. L. FU and I. C. HO, *J. Mater. Sci. Lett.* **8** (1989) 999.
7. S. WAKU, A. NISHIMURA, T. MURAKAMI, A. YAMAJI, T. EDAHIRE and M. UCHIDATE, *Rev. Electr. Commun. Lab.* **9** (1971) 665.
8. P. GAUCHER, R. L. PERRIER and J. P. GENNE, *Adv. Ceram. Mater.* **3** (1988) 273.
9. K. KOSUGE, *J. Phys. Chem. Solids* **28** (1967) 1617.
10. D. N. PATEL and L. WILLIAMS Jr, *Proc. ISHM* Montgomery, AL (1974) p. 477.
11. L. MURAWSKI, C. GLEDEL, C. SANEHEZ, J. LIVAGE and J. P. AUDIERES, *J. Non-Cryst. Solids* **89** (1987) 98.
12. J. DANIELS and R. WERMOCLE, *Philips Res. Rept.* **31** (1976) 544.
13. H. M. AL-ALLAK, G. J. RUSSEL and J. WOODS, *J. Phys. D Appl. Phys.* **20** (1987) 1645.
14. G. J. HYLAND, *J. Solid State Chem.* **2** (1970) 318.
15. J. P. AUDIERE, A. MADI and J. C. GRENET, *J. Mater. Sci.* **17** (1982) 2973.
16. I. C. HO and S. L. FU, *ibid.* in press.
17. D. HENNINGS and A. SCHNELL, *J. Amer. Ceram. Soc.* **65** (1982) 539.
18. R. KOHLMULLER and J. PERRAUD, *Bull. Soc. Chim.* **3** (1964) 644.
19. S. SOLACOLU, R. DINESCU and M. ZAHARESCU, *Rev. Roum. Chim.* **17** (1972) 311.
20. S. SHIRASAKI and H. HANEDA, *J. Mater. Sci.* **22** (1987) 4439.
21. J. P. MEKELVEY, "Solid State and Semiconductor Physics", (Harper and Row, New York, 1971) p. 153.
22. W. HEYWANG, *J. Amer. Ceram. Soc.* **47** (1964) 484.
23. L. C. BURTON, *IEEE Trans Comp. Hyb. Manuf. Technol.* **CHMT 8** (1985) 517.
24. I. K. YEE, L. C. BURTON and F. W. STEPHENSON, *ibid.* **CHMT 10** (1987) 274.

Received 21 February and accepted 26 February 1990